BIOCHEMISTRY
including biophysical chemistry & molecular biology
Article

Biochemistry **2009,** *48,* 4753–4761 4753
DOI: 10.1021/bi900267r

Photosynthetic System in *Blastochloris viridis* Revisited[†]

Marina Konorty,*[,‡] Vlad Brumfeld,[§] Andre Vermeglio,[∥] Nava Kahana,[‡] Ohad Medalia,[⊥] and Abraham Minsky[‡]

[‡]*Department of Organic Chemistry and* [§]*Department of Plant Sciences, The Weizmann Institute of Science, Rehovot 76100, Israel,* [∥]*CEA, DSV, IBEB, Lab Bioenerget Cellulaire, Saint-Paul-lez-Durance F-13108, France, CNRS, UMR Biol Veget & Microbiol Environ, Saint-Paul-lez-Durance F-13108, France, Aix-Marseille Université, Saint-Paul-lez-Durance F-13108, France, and* [⊥]*Ben Gurion University, Beer Sheva 84120, Israel*

Received February 17, 2009; Revised Manuscript Received April 23, 2009

ABSTRACT: The bacterium *Blastochloris viridis* carries one of the simplest photosynthetic systems, which includes a single light-harvesting complex that surrounds the reaction center, membrane soluble quinones, and a soluble periplasmic protein cytochrome c_2 that shuttle between the reaction center and the bc_1 complex and act as electron carriers, as well as the ATP synthase. The close arrangement of the photosynthetic membranes in *Bl. viridis*, along with the extremely tight arrangement of the photosystems within these membranes, raises a fundamental question about the diffusion of the electron carriers. To address this issue, we analyzed the structure and response of the *Bl. viridis* photosynthetic system to various light conditions, by using a combination of electron microscopy, whole-cell cryotomography, and spectroscopic methods. We demonstrate that in response to high light intensities, the ratio of both cytochrome c_2 and bc_1 complexes to the reaction centers is increased. The shorter membrane stacks, along with the notion that the bc_1 complex is located at the highly curved edges of these stacks, result in a smaller average distance between the reaction centers and the bc_1 complexes, leading to shorter pathways of cytochrome c_2 between the two complexes. Under anaerobic conditions, the slow diffusion rate is further mitigated by keeping most of the quinone pool reduced, resulting in a concentration gradient of quinols that allows for a constant supply of theses electron carriers to the bc_1 complex.

Purple photosynthetic bacteria are capable of carrying out photosynthesis using a relatively simple system consisting of well-characterized components. Since the photosynthetic process and machinery in these bacteria are basically similar to those of green plants, they can provide new insights into the evolution of the photosynthetic process and its structure−function relation. The initial steps of photosynthesis, common to photosynthetic bacteria and plants, comprise light absorption and subsequent transfer of the excitation energy to the reaction center (RC),[1] where charge separation takes place. The photochemically induced charge separation drives the ATP-generating machinery and reducing power.

Blastochloris (formerly *Rhodopseudomonas*) *viridis* is a purple photosynthetic bacterium that carries one of the simplest photosynthetic systems in nature. It consists of only one light-harvesting complex (LH) that closely surrounds the RC, two diffusing electron carriers consisting of the membrane soluble hydrophobic quinones, and a soluble periplasmic protein cytochrome c_2, as well as the bc_1 complex and ATP synthase. Energy absorbed by the LH is transferred to the RC. This excitation transfer induces a charge separation between the bacteriochlorophyll special pair in the RC and the primary bound quinone Q_A, leading to an electron transfer to the secondary quinone Q_B. Following a second charge separation, the doubly reduced and protonated Q_B diffuses to the bc_1 complex where it is oxidized with a concomitant transfer of protons from the cytoplasm to the periplasm (*1*). The electrons are then shuttled back to the photooxidized RC special pair bacteriochlorophyll by cytochrome c_2 through the RC cytochrome C subunit, which is present in most purple bacteria. In *Bl. viridis*, it contains four covalently bound heme groups [*c*-559, *c*-552, *c*-556, and *c*-554 (*2*−*4*)].

The photosynthetic machinery in *Bl. viridis* is located in lamellar, stacked photosynthetic membranes in which the proteins are tightly packed into a two-dimensional hexagonal lattice. Extensive electron microscopy and AFM studies (*5*−*8*) of the *Bl. viridis* photosynthetic membranes revealed that the densely packed two-dimensional lattice consists of LH−RC complexes, but the cytochrome bc_1 and the ATP synthase could not be detected. The failure to detect these integral membrane protein assemblies is not unique to *Bl. viridis* but rather general to purple bacteria, including *Rhodopseudomonas palustris* (*9*), *Rhodobacter sphaeroides* (*10*), *Rhodobacter blasticus* (*11*), and *Phaeospirillum molischianum* (*12*). As both the bc_1 and ATP synthase complexes are mandatory for the photosynthetic machinery, and since the bc_1 complex is present in relatively large amounts [with a bc_1 to RC ratio ranging from 1/5 to 1/2 (*13*)], the recurring failure to

[†]These studies were supported by grants from the Israel Science Foundation (to O.M.) and the Minerva Foundation, Germany (to A.M.).

*To whom correspondence should be addressed. Phone: 972-89342003. Fax: 972-89344142. E-mail: marina.konorty@weizmann.ac.il.

[1]Abbreviations: RC, reaction center; LH, light-harvesting complex; Q_A, primary quinone; Q_B, secondary quinone; Bchl *b*, bacteriochlorophyll *b*; F_M, maximum fluorescence yield; F_0, minimal fluorescence yield; Cyt, cytochrome; TEM, transmission electron microscopy.

 Published on Web 04/28/2009

detect these complexes is intriguing. Since the tightly packed crystalline domains of the light-harvesting complexes have been suggested to impair the free diffusion of quinones (*14*), the apparent absence of the bc_1 complex in the membrane two-dimensional lattice highlights an additional fundamental enigma concerned with the connection between the RCs and these complexes (*13*, *15*). The question of how the photosynthetic cycle is maintained has been underscored by recent high-resolution studies on *Bl. viridis*, which demonstrated that in addition to the close lamellar apposition of the photosynthetic membranes, the entire membranal system reveals a crystalline organization (*16*). In *Bl. viridis*, RCs were shown to protrude from both cytoplasmic and periplasmic membranal faces (*8*). These protrusions, along with the close apposition of the photosynthetic membranes and with the tight two-dimensional crystalline arrangement of the RC−LH complexes, result in highly crowded membranal and cellular milieus that are likely to significantly affect the diffusion processes. Indeed, the issue of electron carrier diffusion within crowded photosynthetic membranes remains elusive and continues to attract much interest (*13*, *14*, *16*−*18*).

To gain insight into the functional organization in the *Bl. viridis* photosynthetic system and how it efficiently operates regardless of the above-mentioned characteristics, we have studied the formation, architecture, and mode of operation of the photosynthetic membrane system in this bacterium. We followed the maturation of the photosynthetic membrane and investigated the effects of light intensity on the organization of the photosynthetic apparatus and the photosynthetic cyclic electron transfer. On the basis of our observations, we propose a possible location of the cytochrome bc_1 complex and ATP synthase. Moreover, our observations provide a possible solution to the enigmatic mode of diffusion within the tightly packed photosynthetic membranes.

MATERIALS AND METHODS

Bacterial Strains and Growth Conditions. *Bl. viridis* bacteria were grown anaerobically in liquid cultures in yeast medium for *Rhodospirillaceae*. The medium consisted of 0.5 g of KH_2PO_4, 0.4 g of $MgSO_4$, 0.4 g of NaCl, 0.4 g of NH_4Cl, 0.05 g of $CaCl_2$, 1.5 g of malic acid, 2 g of yeast extract, 6 mL of iron citrate solution, and 1 mL of a trace element solution, per liter (pH 6.9). The trace element solution consisted of 0.1 g of $ZnSO_4 \cdot 7H_2O$, 0.03 g of $MnCl_2 \cdot 4H_2O$, 0.3 g of H_3BO_3, $CoCl_2 \cdot 6H_2O$, 0.01 g of $CuCl_2 \cdot 2H_2O$, 0.02 g of $NiCl_2 \cdot 6H_2O$, and 0.03 g of $NaMoO_4 \cdot 2H_2O$, per liter. The iron citrate solution consisted of 0.3 g of $FeSO_4$, 0.26 g of $(NH_4)_2SO_4$, and 0.84 g of citric acid, per 500 mL. For studies of photosynthetic membrane induction, cells were grown for 2 days in the dark, inoculated in fresh medium, and kept in the dark for an additional 2 days prior to illumination. Cells were illuminated at a light intensity of 300 μE m^{-2} s^{-1}. High-light-adapted bacteria were grown following dark adaptation for 1 day at a light intensity of 120 μE m^{-2} s^{-1} and then for 2 days at 300 μE m^{-2} s^{-1}. Low-light-adapted bacteria were grown following dark adaptation for 1 day at a light intensity of 120 μE m^{-2} s^{-1} and then for 2 days at 0.7 μE m^{-2} s^{-1}.

Photosynthetic Membrane Isolation. Cells were harvested by centrifugation (11000*g*, 10 min, 4 °C) and resuspended in 30 mL of 10 mM Tris-HCl (pH 7.5). Following addition of antiproteases and PMSF (250 μM), cells were disrupted with a French press at 16000 psi. The homogenate was then centrifuged to remove cell debris and unbroken cells (SS-34, 20000*g*, 4 °C). The membrane fraction was obtained by sedimentation (215000*g*, 30 min, 4 °C), resuspended in Tris-HCl (pH 7.5), loaded on a 10 to 60% sucrose gradient, and centrifuged at 110000*g* for 15 h at 4 °C.

Other Procedures. SDS−PAGE was carried out on 12% polyacrylamide gels subsequently stained with Commassie blue or heme staining according to the method of Thomas et al. (*19*). Western blots for cytochrome c_1 detection were probed with two different rabbit polyclonal antibodies: antibodies raised against *Rb. sphaeroides* cytochrome c_1 that were a gift from C.-A. Yu (Oklahoma State University, Stillwater, OK) and antibodies raised against *Bl. viridis* cytochrome c_1. The concentration of bacteriochlorophyll *b* (Bchl *b*) in isolated membranes was determined after extraction with an acetone/methanol mixture (7:2, v/v), using an extinction coefficient of 122 mM^{-1} cm^{-1} at 790 nm following the method of Garcia et al. (*20*). Bchl *b* determination in cells was performed by its extraction with methanol according to the method of Lang and Osterhelt (*21*) using a molar extinction coefficient of 96 mM^{-1} cm^{-1}. Protein concentrations were determined by the Bradford method.

Electron Microscopy. *(i) Negative Stain Electron Microscopy*. For negative stain transmission electron microscopy (TEM) imaging, isolated photosynthetic membranes were washed with 10 mM Tris-HCl, applied to glow-discharged 200-mesh carbon-coated grids, and negatively stained with 1% uranyl acetate (UrAc). Samples were examined on a Tecnai T-12 (FEI) electron microscope equipped with a SIS MegaView III CCD camera and operated at 120 kV.

(ii) Cryo-TEM and Cryoelectron Tomography. A 5 μL drop of bacteria solution was applied onto glow-discharged 200-mesh carbon-coated copper grids (Quantifoil, Jenna) and vitrified (*22*). For cryotomography, homemade 15 nm colloidal gold was added before vitrification. Data were collected using a 300 kV FEI Polara (FEI) transmission electron microscope equipped with a field-emission gun, and a Gatan postcolumn GIF 2002 energy filter. Tilt series were collected over an angular range of 66° to −66°, with a 2° increment. Defocus values ranged from −12 to −16 μm. The resulting pixel size was 0.8−11 Å at the specimen level. The micrographs were aligned to a common origin using the fiducial gold markers. To minimize systematic alignment errors, gold markers in the closest vicinity of a membrane stack were kept fixed in a least-squares fit as implemented by the TOM package (*23*). Subsequently, three-dimensional reconstructions were computed by means of weighted back-projection using the EM image-processing software package (*24*).

Image Processing. Membranes within the reconstructed volumes were segmented manually. Segmentation was performed with denoised volumes [using the nonlinear anisotropic diffusion algorithm (*25*)] to prepare binary volume masks of the region of interest. The masks were then multiplied with the original data to give segmented volumes that exhibit resolution identical to that of the original data. The segmented volumes were visualized by the Amira 4.1 (Mercury Computer Systems) surface rendering modules.

Fluorescence Measurements. For fluorescence induction kinetics measurements, a double-modulated fluorometer (Fluorwin 3300, PSI, Brno, Czech Republic) was used. Excitation was induced using a 455 nm LED matrix, and fluorescence emission was collected through an 800 nm long pass filter and measured with a photodiode. Fluorescence induction kinetics were measured by applying a saturating pulse (120 μs at 455 nm) to the sample during which fluorescence was sampled with high

Table 1: Bacteriochlorophyll *b* Concentration in *Bl. viridis* Cells

culture conditions[a]	bacteriochlorophyll *b* (nmol/g of cells)[b]
anaerobic, dark	not detected
anaerobic, light for 24 h	not detected
anaerobic, light for 48 h	7 ± 1
anaerobic, light for 54 h	50 ± 7
anaerobic, light for 72 h	330 ± 35
anaerobic, light for 96 h	245 ± 20

[a] *Bl. viridis* cells were dark-adapted and then illuminated at 300 μE m^{-2} s^{-1}. [b] Values represent an average of four measurements.

frequency (100 ns). The measurement allowed accurate estimation of the quantum yield of photochemistry via the equation $(F_M - F_0)/F_M = F_V/F_M$, where F_M is the maximum fluorescence yield and F_0 is the minimal fluorescence yield in whole bacteria grown under different light intensities. Prior to measurements, samples were dark-adapted at room temperature under anaerobic conditions for 15 min.

Time-Resolved Absorption Measurements. Light-induced absorbance changes were preformed on an apparatus similar to the one described by Joliot et al. (*26*) and modified according to ref *27*. In the case of aerobic conditions, air was gently bubbled into the cell suspension. Anaerobiosis was achieved by dark adaptation for 15 min at room temperature. Actinic excitation light was provided by a xenon lamp (3 μs half-time pulses) or a 12 V quartz-halogen lamp. Cytochrome c_2 photooxidation and re-reduction were assessed by monitoring the absorbance change at 550 nm. Photooxidation and re-reduction kinetics of cytochrome *c*-556 were measured by monitoring absorbance changes at 558 nm.

RESULTS

To study the induction and development of the photosynthetic membrane system in *Bl. viridis,* cells were transferred from anaerobically dark to anaerobically light conditions. The cellular morphology was investigated at defined time points following the shift to light using whole-mount cryoelectron tomography. In addition, the cellular Bchl *b* concentration, which reflects the sum of the concentration of LH complexes and RCs (*21*), was monitored.

Dark-adapted *Bl. viridis* cells (obtained as described in Materials and Methods) are completely devoid of intracytoplasmic photosynthetic membranes, consistent with the absence of Bchl *b* in these cells (Table 1). Following illumination for 48 h at 300 μE m^{-2} s^{-1}, synthesis of photosynthetic proteins is induced, as indicated by the increase in the Bchl *b* concentration. This induction correlates with the appearance of cell membrane invaginations (Figure 1A) and small vesicle-like structures (Figure 1B), which can be detected mainly at the vicinity of the cell poles. As the level of Bchl *b* increases, the amount and size of the membrane invaginations increase as well. Stacking is often observed between two cytoplasmic face membranes of two such structures (Figure 2A,B). The cellular concentration of Bchl *b* reaches its highest levels between 72 and 96 h of illumination, and concomitantly, the photosynthetic membranes rearrange into their characteristic morphology (*28*) of partially stacked thylakoids, adjacent to the cell membrane (Figure 2C,D). The disassembly of photosynthetic membranes following transfer to dark conditions was found to be very slow, as more than 10%

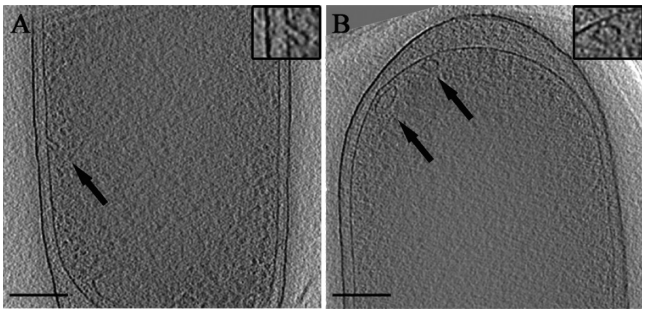

FIGURE 1: Cryoelectron tomography of intact *Bl. viridis* cells illuminated for 48 h. 10 nm thick $x-y$ slices through typical cryoelectron tomograms of intact *Bl. viridis* cells illuminated for 48 h at 300 μE m^{-2} s^{-1} are shown. Arrows indicate small invaginations (A) and vesicle-like structures (B). Insets show the enlargement of the indicated areas. Bars are 200 nm.

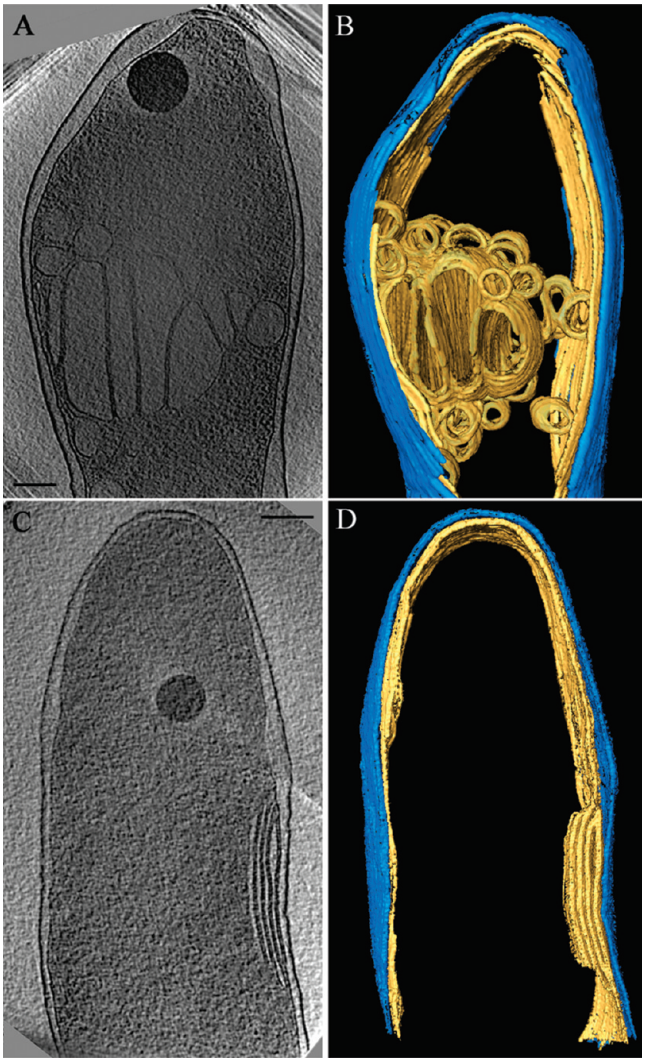

FIGURE 2: Cryoelectron tomography of intact *Bl. viridis* cells in the process of de novo photosynthetic membrane generation. (A and B) Cells illuminated for 54 h at 300 μE m^{-2} s^{-1}. (A) A 13 nm thick $x-y$ slice through the cell tomogram. (B) Surface-rendered view of the cell shown in panel A, where photosynthetic membranes and the plasma membrane are colored yellow and the cell wall is colored blue. (C and D) Cells illuminated for 96 h at 300 μE m^{-2} s^{-1}. (C) A 4.5 nm thick $x-y$ slice through the cell tomogram. (D) Surface-rendered view of the cell shown in panel C, where the photosynthetic membrane and the plasma membrane are colored yellow and the cell wall is colored blue. Bars are 200 nm.

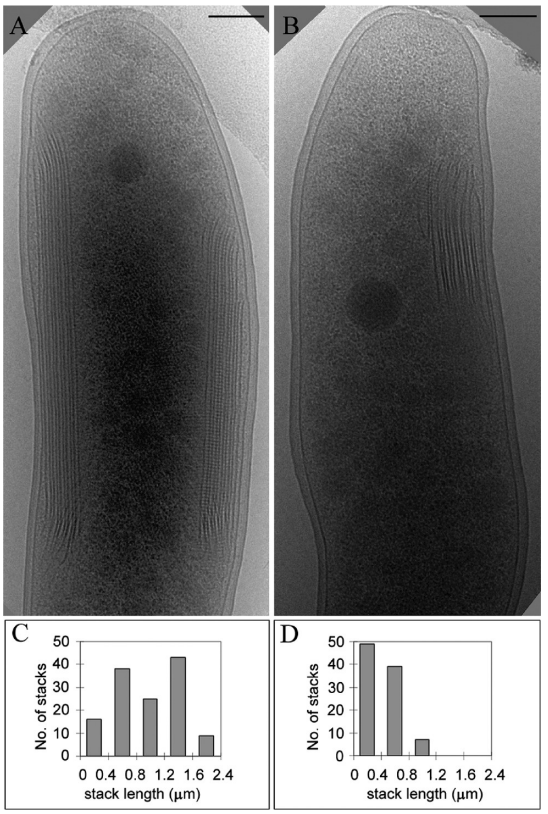

FIGURE 3: Structure and size analysis of the photosynthetic membranes in high- and low-light-adapted cells. (A and B) Transmission electron micrographs of a typical low-light-adapted *Bl. viridis* cell (A) and of a high-light-adapted *Bl. viridis* cell (B). Bars are 200 nm. (C and D) Distribution of photosynthetic membrane stack lengths in low-light-adapted (C) and high-light-adapted (D) cells.

of the population still maintains intracellular membranes even after 48 h.

Structural Analysis of High- and Low-Light-Adapted Cells. Representative cryo-TEM images of high (300 μE m^{-2} s^{-1})- and low (0.7 μE m^{-2} s^{-1})-light intensity-adapted *Bl. viridis* cells are shown in Figure 3. Low-light-adapted cells are characterized by relatively long stacks of highly ordered membranes. Analysis of >100 cells revealed an average of 1 μm long ($\pm$0.45 μm) photosynthetic membrane stacks, composed of 18 ($\pm$6) stacked photosynthetic membranes. In contrast, the average length of the photosynthetic membrane stacks in high light-adapted cells is 0.45 μm ($\pm$0.23 μm), with an average of 12 ($\pm$6) stacked membranes.

To compare the composition and architecture of the photosynthetic membranes in high- and low-light-adapted cells, we isolated photosynthetic membranes from these cells. Membranes derived from both populations are found to contain equal concentrations of Bchl *b* (33 nmol/mg of protein). To confirm the presence of the bc_1 complex following membrane isolation, Western blot analysis was conducted with polyclonal antibodies raised against subunit c_1 of the *Rb. sphaeroides* cytochrome bc_1 complex (provided by C.-A. Yu). Since this antibody was found to cross-react with *Bl. viridis* RC cytochrome C subunit, it is unsuitable for in situ immuno-gold labeling experiments, yet adequate for Western blots analysis, and for estimation of the dependence of the bc_1/RC ratio on illumination conditions. Figure 4C,D shows a densitometer trace of Western blots of membranes isolated from high- and low-light-adapted cells. Both cytochrome C subunit and Cyt c_1 were identified by their corresponding molecular masses (38 and 31 kDa, respectively) as well as by heme staining. The bc_1/RC ratio was found to be ~2 times higher in high-light-adapted cells, confirming previous observations on *Bl. viridis* (*29*) and *Rhodobacter capsulatus* (*30*).

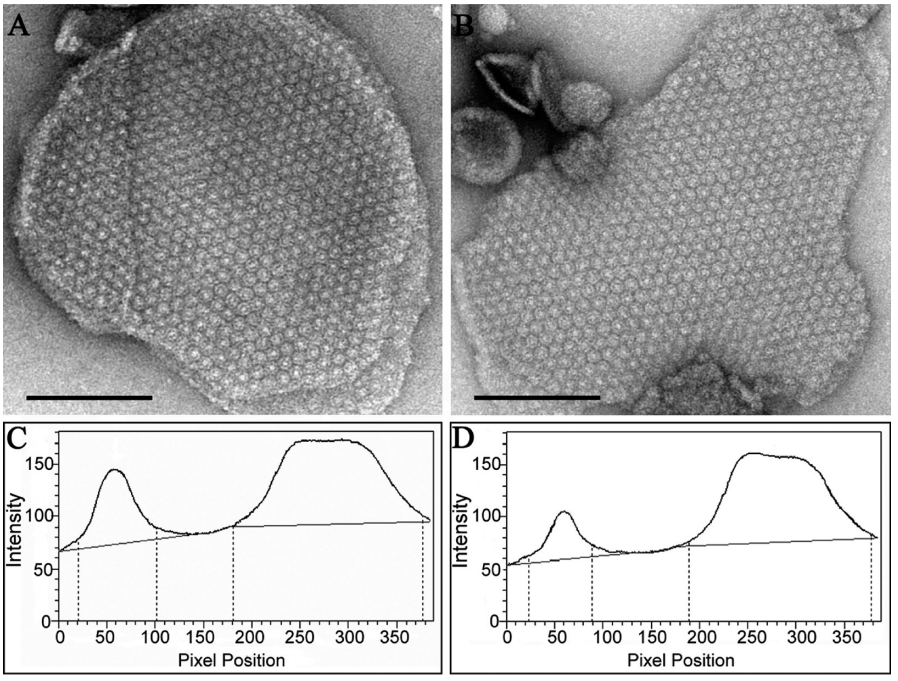

FIGURE 4: Electron microscopy and Western blot against cytochrome c_1 of photosynthetic membranes isolated from high- and low-light-adapted *Bl. viridis* cells. (A and B) TEM images of negatively stained isolated membrane, isolated from high-light-adapted (A) and low-light adapted (B) cells. The bar is 100 nm. (C and D) Densitometer trace of Western blots against *Rb. sphaeroides* cytochrome c_1 in isolated membranes of bacteria grown in high (C) and low (D) light intensities. The intensity depicted at pixel position 20-90 represents interaction of the anti-c_1 antibody with Cyt c_1, whereas the intensity at pixel position 190-380 represents cross reaction with the RC cytochrome C subunit.

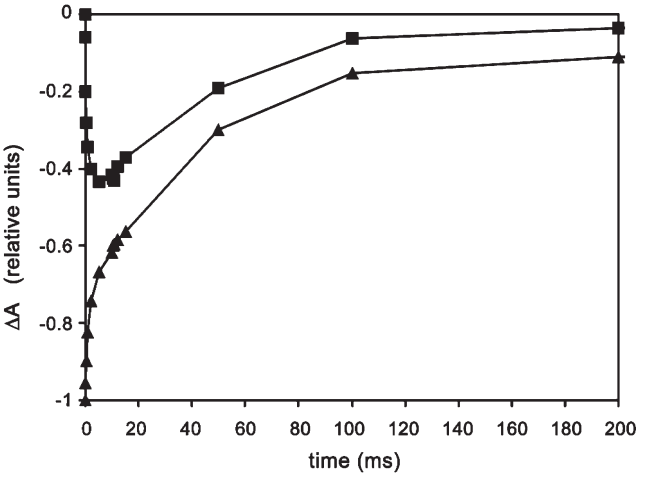

FIGURE 5: Electron transfer in *Bl. viridis* cells in the process of photosynthetic membrane generation. Kinetics of oxidation and re-reduction of cytochrome c_2 and *c*-556 RC's heme, in cells during the process of photosynthetic membrane generation (54 h illumination). Cytochrome c_2 kinetics measured at 550 nm (■). *c*-556 kinetics measured at 558 nm (▲). Measurements were performed under anaerobic conditions.

Isolated membranes were further investigated by electron microscopy (Figure 4A,B). Irrespective of illumination conditions, membranes were found to be highly packed with straightforwardly identified reaction centers. However, no additional assemblies such as the bc_1 complex and ATP synthase could be detected in these high-resolution studies, in contrast to our finding derived from Western blot analysis which indicates the presence of the bc_1 complex (Figure 4B,C). This apparent contradiction will be discussed below. In addition, we tried to determine the in situ location of the bc_1 complex within the photosynthetic membrane using polyclonal antibodies raised against the isolated cytochrome c_1 subunit of the *Bl. viridis* bc_1 complex [in contrast to the antibodies described above which were raised against the *Rb. sphaeroides* c_1 subunit (see the Supporting Information)]. The high specificity of the anti-c_1 antibody [indicated by the Western blot (Figure S1 of the Supporting Information)] notwithstanding, no labeling of the bc_1 complex was obtained.

Kinetics of Cyclic Electron Transfer in Whole Cells. The kinetics of photosynthetic electron transfer was studied by light-induced absorbance changes in whole, intact *Bl. viridis* cells during de novo photosynthetic membrane development, as well as in high- and low-light-adapted cells. We measured the kinetics of electron transfer between cytochrome c_2 and the RC high-potential cytochrome *c*-556 and their re-reduction process, by monitoring light-induced absorbance changes at 550 nm (c_2) and 558 nm (*c*-556) (*31*, *32*) following excitation with a single saturating pulse. From the kinetics of c_2 re-reduction, one can derive the completion of the electrogenic reaction in the bc_1 complex. Experiments performed under anaerobic conditions (where the quinol pool is largely reduced) were conducted under a continuous background low-intensity illumination. This background illumination ensured photooxidation of the low-potential hemes of the RCs, and partial oxidation of the quinol pool. Figure 5 shows the kinetics of 54 h-illuminated cells measured under these conditions. Notably, at this time point, cells are in the process of photosynthetic membrane development. The *c*-556 re-reduction reveals two phases. The first phase is completed in 2 ms and correlates with cytochrome c_2 photooxidation. The half-time

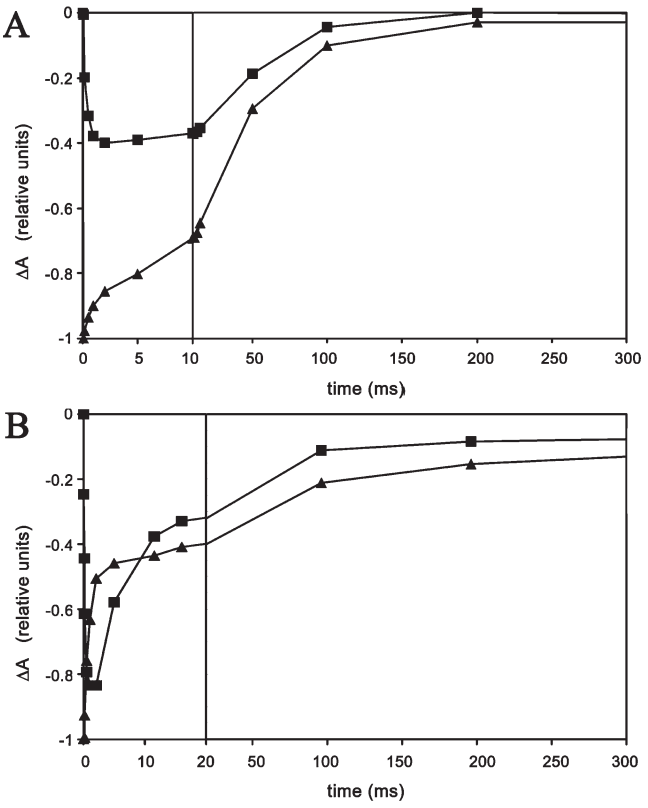

FIGURE 6: Electron transfer in low- and high-light-adapted *Bl. viridis* cells. Kinetics of oxidation and re-reduction of cytochrome c_2 and *c*-556 RC's heme, in low-light-adapted (A) and high-light-adapted (B) *Bl. viridis* cells measured under anaerobic conditions. Cytochrome c_2 kinetics measured at 550 nm (■). *c*-556 kinetics measured at 558 nm (▲). Note the different time scales (separated by black lines).

of the second phase is 48 ms and correlates with the re-reduction phase of c_2.

Figure 6 depicts *c*-556 and c_2 kinetics in high- and low-light-adapted cells, measured under similar experimental conditions. Electron transfer kinetics in low-light-adapted cells (Figure 6A) is reminiscent of the kinetics revealed by 54 h-illuminated cells. In particular, the re-reduction kinetics of cytochrome c_2 is monophasic with a half-time of 48 ms and correlates with the second phase of the *c*-556 re-reduction. In contrast, the high-light-adapted cells differ from 54 h-illuminated cells, as clear biphasic kinetics of cytochrome c_2 re-reduction is revealed (Figure 6B). The first phase is fast, with a half-time of 5 ms (completed in 16 ms), whereas the second re-reduction phase reveals a half-time of 80 ms. Both phases correlate with cytochrome *c*-556 re-reduction.

We next measured the kinetics of cytochrome *c*-556 and c_2 in low-light-adapted cells under aerobic conditions (Figure 7). Under such conditions, most of the quinol pool is oxidized (*33*). Cytochrome c_2 re-reduction is slower than under anaerobic (reducing) conditions with a half-time of 186 ms. This slow re-reduction correlates with a slow *c*-556 re-reduction characterized by a half-time of 155 ms. Therefore, changing the redox conditions of the low-light-adapted cells from anaerobic to aerobic slowed cytochrome c_2 and *c*-556 re-reduction by a factor of ~4 (Figures 6A and 7).

The aforementioned results demonstrate that reduction of 90% of c_2 following a saturation flash under reducing conditions requires approximately 100 ms. The kinetics of the cyclic electron

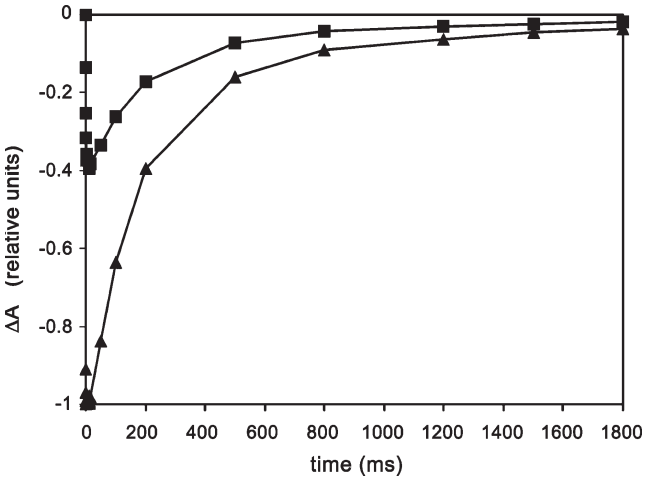

FIGURE 7: Electron transfer in low-light-adapted *Bl. viridis* cells. Kinetics of oxidation and re-reduction of cytochrome c_2 and *c*-556 RC's heme, in low-light-adapted *Bl. viridis* cells measured under aerobic conditions. Cytochrome c_2 kinetics measured at 550 nm (■). *c*-556 kinetics measured at 558 nm (▲).

transfer in *Bl. viridis* is thus 20 times slower than in *Rb. sphaeroides* (*34*), 10 times slower than in *Rb. capsulatus* (*35*), and 2 times slower than in *Rhodospirillum rubrum* (*36*). An additional result derived from the above data is the relative ratios between the total photooxidizable c_2 and cytochrome *c*-556 in *Bl. viridis* cells during the process of de novo photosynthetic membrane development, as well as in high- and low-light-adapted cultures. Comparison of the maximal absorbance changes of cytochrome *c*-556 and of c_2 reveals that the c_2/*c*-556 (c_2/RC) ratio in high-light-adapted cells is twice as high as in low-light-adapted cells (Figure 6). In contrast, the c_2/*c*-556 ratio (c_2/RC) in *Bl. viridis* cells undergoing photosynthetic membrane development is only 10% higher than that in low-light-illuminated cells.

Fluorescence Measurements. To study the extent of functionality of the reaction centers in *Bl. viridis* cells, at their three examined states (de novo photosynthetic membrane development and high- and low-light-adapted cells), we have measured the quantum yield of the primary charge separation, calculated by $F_V/F_M = (F_M - F_0)/F_M$. Our results indicate that F_V/F_M values are practically identical for high- and low-light-adapted cells (0.73 and 0.75, respectively), yet lower (0.64) for cells that are in the process of membrane development.

DISCUSSION

Developmental Aspects. When grown in the dark, *Bl. viridis* cells do not contain inner cellular membranes (ICMs), and no indentations of the cell membrane could be detected. These observations are in contrast with those for *Rb. sphaeroides* cells where such indentations, which could act as initiation sites for ICM development, have been reported (*37*−*39*). On the basis of our results, we suggest that the progression of ICM formation entails several sequential steps (Figure 8). The process is initiated by cell membrane invaginations that are detected exclusively at the cell poles (Figure 1). The spatial correlation between invaginations and cell poles is intriguing in light of the growing realization that the curvature at bacterial pole sites represents a major factor in lipid and protein localization, acting as such as a symmetry-breaking element (*40*). The continuity between the invaginations and the cell membrane could not always be

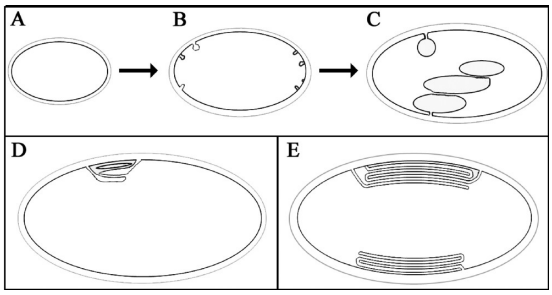

FIGURE 8: Schematic representation of photosynthetic membrane morphology in *Bl. viridis* cells. (A−C) Sequential morphological events at the membrane level during de novo generation of photosynthetic membranes. (D and E) Membrane organization in high-light-adapted (D) and low-light-adapted (E) cells.

detected, presumably because of their intrinsically low contrast and the high density of the cellular milieu. In the following stage, the invaginations drastically grow in size and swell into spherical vesicle-like structures until they collide with enlarging adjacent invaginations (Figure 2A,B). These collisions promote stacking between the cytoplasmic faces of apposed membranes. During the last stage of light adaptation, the vesicle-like structures become flattened, stacking appears also at their periplasmic face, and the mature stacks become localized in the proximity of the cell membrane (Figure 2C,D).

The sequential formation of ICMs in *Bl. viridis* contrasts to ICM generation in other species. In the purple non-sulfur bacterium *Rs. palustris*, ICM synthesis is initiated through cell membrane invaginations that, in contrast to those in *Bl. viridis*, do not evolve into large spherical structures but rather progress directly into mature tightly stacked thylakoids, remaining flat and apposed to the cytoplasmic membrane throughout morphogenesis (*41*). In the purple non-sulfur bacteria *Rb. sphaeroides* and *Rsp. rubrum,* mature ICMs adopt a vesicular morphology (*37*) similar to that revealed by *Bl. viridis* in the intermediate stage of ICM development (Figure 8C).

In addition to the difference in the ICM morphogenesis between *Bl. viridis* and other photosynthetic bacteria, we find that the response time to illumination significantly varies in the various species. Upon a dark-to-light shift, *Bl. viridis* cells initiate ICM generation after 48 h, whereas *Rb. sphaeroides* or *Rsp. rubrum* initiates ICMs synthesis within 1 h (*37*) or 18−24 h (*42*), respectively, which likely implies a general slower adaptation rate of *Bl. viridis*.

The morphology of the mature photosynthetic membrane stack depends on illumination conditions. To assess this final state, our experiments were conducted on bacteria adapted to high or low light intensity. Whereas the membrane internal structure and the quantum yield were similar at both light intensities, membrane stacks are shorter in bacteria grown at high light intensity than in low-light-adapted cells (Figures 3 and 8D,E), implying that the photosynthetic membrane surface is at least twice as long in low-light-adapted as in high-light-adapted cells. Expansion of ICMs as a response to light intensity downshift has been reported for other photosynthetic organisms such as *Rb. capsulatus*, *Rb. sphaeroides*, and *Rsp. rubrum* (*43*, *44*) and is reminiscent of the adaptation of the grana domain in green plants to different light intensities (*45*, *46*). We also find that membrane stacks in high-light-adapted cells are considerably less ordered than in the low-light-adapted cells (Figure 3).

Western blots of membranes isolated from high- and low-light-adapted cells using antibodies against the bc_1 subunit cytochrome

c_1 (from *Rb. sphaeroides*) indicated a higher bc_1/RC ratio in high-light-adapted bacteria (Figure 4C,D). This observation is consistent with the work of Cully et al. (*29*) for *Bl. viridis*, and with the observations of Garcia et al. (*30*) for *Rb. capsulatus*, yet photosynthetic membranes isolated from bacteria grown under both high and low light intensities revealed an identical organization (Figure 4A,B), with a straightforwardly identified RC. Notably, the tight and ordered packaging of the RCs leaves no free space for other large, membrane assemblies such the bc_1 complex or ATP synthase [~10 and 5.5 nm in diameter, respectively (*47*, *48*)]. The highly occupied photosynthetic membrane, as well as the failure to detect complexes besides the RC and LH, is consistent with AFM studies conducted on *Bl. viridis* (*8*), *Rhodospirillum photometricum* (*49*), *Rb. sphaeroides* (*10*), *Rb. blasticus* (*11*), and *Phsp. molischianum* (*12*). Following the failure to detect the bc_1 complex, it has been suggested that the bc_1 might be located close to, or at the junction with, the cytoplasmic membrane (*49*).

We have attempted to label the bc_1 complex in sections of high-pressure-frozen, freeze-substituted cells, and in isolated photosynthetic membrane, with antibodies raised against cytochrome c_1 isolated from *Bl. viridis*, yet failed to obtain specific labeling. The reason for this failure, in spite of the high specificity of the anti-c_1 antibody (see the Supporting Information), remains unclear, highlighting again the enigmatic intracellular location of the bc_1 complex. We would like, however, to suggest that the bc_1 complex and ATP synthase are located at the highly curved edges of the photosynthetic membrane stacks. This suggestion is based on the following arguments: The presence of bc_1 and ATP synthase at particular membranal locations results in enhanced inhomogeneity at these sites, which might in turn be the cause for the large curvature detected at membrane edges (*50*−*54*). In addition, since highly curved membranal segments are refractory to microscopic analyses (both TEM and AFM), the presence of bc_1 and ATP synthase at such sites might provide a rationale for their failure to be detected.

Notably, as the connections of the photosynthetic membrane to the cell membrane in *Bl. viridis* are regularly found near the photosynthetic stack edges (*16*), both suggestions for bc_1 intracellular location imply that the overwhelming majority of the RCs is located away from the bc_1 complexes. This is particularly evident in *Bl. viridis* cells grown at low light intensities since the surface of the photosynthetic membranes in these cells is larger than in the high-light-adapted cells. It follows that high- and low-light-illuminated cells should reveal a difference in the kinetics of the photosynthetic cyclic electron transfer. To address this issue, we have monitored the rates of the kinetics of cyclic electron transfer in whole cells at the three examined states: in the process of de novo photosynthetic membrane generation (54 h) as well as in high- and low-light-adapted cells.

Kinetics of Cyclic Electron Transfer in Whole Cells. Our measurements of the RC high-potential heme *c*-556 and cytochrome c_2 photooxidation and re-reduction kinetics indicate that the photosynthetic cycle in *Bl. viridis* is significantly slower than in other bacteria such as *Rb. sphaeroides and Rb. capsulatus* (*34*, *35*). The slower kinetics of *Bl. viridis* can be straightforwardly assigned to the relatively low bc_1/RC ratio [0.2 vs 0.5 for *Rb. sphaeroides and Rb. capsulatus* (*55*, *56*)], as well as to the spatial separation between the bc_1 complex and the RCs that contrasts the suggested supercomplex organization of the photosystems in *Rb. sphaeroides and Rb. capsulatus* (*35*, *57*−*64*). The slow kinetics of *Bl. viridis* enables the separation of different phases of the cyclic electron transfer and highlights the tight correlation between cytochrome *c*-556 and cytochrome c_2 kinetics.

Specifically, *c*-556 re-reduction in *Bl. viridis* appears as a multiphasic process. Under anaerobic conditions and irrespective of the growth conditions, the first phase of *c*-556 re-reduction is the fastest phase and correlates with cytochrome c_2 photooxidation. The tight correlation between this fast phase and c_2 photooxidation for cells grown under the various conditions indicates that c_2 forms a stable complex with the RC tetraheme, in agreement with previous results (*32*). Comparison of the maximal absorbance changes of cytochrome *c*-556 and of c_2 at the end of this phase reveals that the c_2/*c*-556 (c_2/RC) ratio in high-light-adapted cells is twice as large as in low-light-adapted cells. Under the conditions used, most of the quinone pool is reduced and the cyclic electron transfer is limited by the electron transfer between the bc_1 complex and the RC via cyt c_2. In contrast to low-light-adapted cells, cytochrome c_2 re-reduction kinetics in high-light-adapted cells is biphasic (Figure 6), presenting an additional fast phase with a half-time of 5 ms. We suggest that this c_2 re-reduction fast phase is related to the higher protein ratios (c_2/RC and bc_1/RC) and to the structural differences in the photosynthetic membrane systems between the high- and low-light-adapted cells. If indeed there is a shorter distance between the bc_1 complex and the RC in high-light-adapted cells, as suggested from our structural results, the diffusion time of the c_2 between the two complexes is likely to be shorter in the high-light-adapted cells than in the low-light-adapted cells. Consequently, c_2 re-reduction will be faster, as indeed observed.

Under aerobic conditions, most of the quinone pool is oxidized, and hence, there is a shortage in reduced quinones (QH_2) that can be oxidized by the bc_1 complex. The c_2 re-reduction process is limited by the diffusion of the quinols formed at the RC level. This process is slowed by a factor of 4 under aerobic conditions in comparison with anaerobic conditions, thus indicating that under aerobic conditions the rate of the cyclic electron transfer is limited by the diffusion of quinol molecules in the membrane.

Cells grown under low- and high-light conditions exhibit different membrane architecture and ratios of photosynthetic proteins. These differences, but not a different activity of the reaction centers ($F_V/F_M \sim 0.75$ for both illumination conditions), are responsible for the increased photosynthetic activity in high-light-adapted cells. In addition, no evidence of an effectively higher antenna area in low-light-adapted cells was found (data not shown), implying that the possibility that part of the photosystems serves only for excitation transfer is unlikely.

The activity level of cells in the process of de novo photosynthetic membrane generation (54 h) is between the levels revealed by low- and high-light-adapted cells. Although illuminated with the same light intensity as high-light-adapted cells (300 μE m^{-2} s^{-1}), cells in the process of membrane generation reveal different kinetics. This observation can be readily reconciled with our measured quantum yield of the primary charge separation (F_V/F_M), which was lower for these cells than that of light-adapted cells, implying that in developing cells the photosynthetic system (RCs) is not yet fully active. This is also reflected in the c_2/RC ratio, which is significantly lower in developing cells than in high-light-adapted cells. Accordingly, the cyclic electron transfer is slower than in high-light-adapted cells and resembles the kinetics of low-light-adapted cells.

Specifically, in both cultures (54 h-illuminated cells and low-light-adapted cells) c_2 re-reduction kinetics is monophasic and the half-time of the kinetics is almost identical (46−48 ms). The notion of a nonmature state of the 54 h-illuminated cells is strongly supported by our morphological studies, according to which the photosynthetic membrane system did not yet reach the characteristic mature stacked structure.

Taken together, these observations and considerations provide the following insights. *Bl. viridis* adjusts its photosynthetic system in response to illumination conditions. A clear correlation is found between the photosynthetic activity and the overall architecture of the photosynthetic membranes. High-light-adapted cells are characterized by high activity, which is reflected by high c_2/RC and bc_1/RC ratios, and by the relative disordered and shorter photosynthetic membrane stacks. These traits are responsible for the faster electron transfer kinetics found in these cells, enabling their photosynthetic system to cope with high rates of electrons entering the photosynthetic cycle. The relatively low c_2/RC and bc_1/RC ratios as well as the higher order and tighter organization of the ICM system revealed by the low-light-adapted cells are consistent with the low activity revealed by these cells. This aspect is of interest in light of previous studies, which demonstrated that an increased molecular order is a general trend in cells characterized by low metabolic activity (*65*).

In spite of the compositional differences between membranes isolated from high- and low-light-adapted cells, we find that the membrane internal structure characterized by tight and ordered packaging of the RCs, with no free space for other membrane assemblies such the bc_1 complex or ATP synthase, is identical under both high- and low-light conditions. The shorter photosynthetic membrane stacks that characterize high-light-adapted cells, in conjunction with our suggestion that the bc_1 complex is located at the highly curved edges of the stacks, will result in a smaller average distance between the RCs and the bc_1 complexes, leading to shorter pathways of the electron carriers between the two complexes.

The predicament associated with the slow diffusion rates within the highly packed membrane crystalline domains is partially mitigated by keeping most of the quinone pool reduced under anaerobic conditions. A steady state can thus be envisioned, whereby a concentration gradient of the QH_2 is maintained, resulting in a small but constant supply of quinols to bc_1. In such a way, the bc_1 complex does not need to await a particular QH_2 formed at the RC to reduce cytochrome c_2. Moreover, the establishment of a steady state renders the diffusion of electron carriers as a non-rate-limiting step.

ACKNOWLEDGMENT

We thank Prof. Jerome Lavergne (DSV, IBEB, Lab Bioenerget Cellulaire, CEN Cadarache, Saint-Paul-lez-Durance, France) and Prof. Hugo Scheer (Dept. Biologie I, Universitaet Muenchen, Munich, Germany) for their helpful insights.

SUPPORTING INFORMATION AVAILABLE

Additional experimental procedures and Figure S1. This material is available free of charge via the Internet at http://pubs.acs.org.

REFERENCES

1. Lancaster, C. R. D., Ermler, U. E., and Michel, H. (1995) The structures of photosynthetic reaction center from purple bacteria as revealed by X-ray crystallography. In *Anoxygenic photosynthetic bacteria* (Blankenship, R. E., Madigan, M. T., and Bauer, C. E., Eds.) pp 503−526, Kluwer Academic Publishers, Dordrecht, The Netherlands.
2. Nitschke, W., and Rutherford, A. W. (1989) Tetraheme cytochrome C subunit of *Rhodopseudomonas viridis* characterized by EPR. *Biochemistry 28*, 3161–3168.
3. Dracheva, S. M., Drachev, L. A., Konstantinov, A. A., Semenov, A., Skulachev, V. P., Arutjunjan, A. M., Shuvalov, V. A., and Zaberezhnaya, S. M. (1988) Electrogenic steps in the redox reactions catalyzed by photosynthetic reaction-centre complex from *Rhodopseudomonas viridis*. *Eur. J. Biochem. 171*, 253–264.
4. Vermeglio, A., Richaud, P., and Breton, J. (1989) Orientation and assignment of the four cytochrome hemes in *Rhodopseudomonas viridis* reaction centers. *FEBS Lett. 243*, 259–263.
5. Miller, K. R. (1979) Structure of a bacterial photosynthetic membrane. *Proc. Natl. Acad. Sci. U.S.A. 76*, 6415–6419.
6. Welte, W., and Kreutz, W. (1985) Structure of thylakoids in cells of *Rhodopseudomonas viridis* as influenced by growth conditions. *Arch. Microbiol. 141*, 325–329.
7. Engelhardt, H., Baumeister, W., and Saxton, W. O. (1983) Electron microscopy of photosynthetic membranes containing bacteriochlorophyll *b*. *Arch. Microbiol. 135*, 169–175.
8. Scheuring, S., Seguin, J., Marco, S., Levy, D., Robert, B., and Rigaud, J. L. (2003) Nanodissection and high-resolution imaging of the *Rhodopseudomonas viridis* photosynthetic core complex in native membranes by Atomic Force Microscopy. *Proc. Natl. Acad. Sci. U.S.A. 100*, 1690–1693.
9. Scheuring, S., Goncalves, R. P., Prima, V., and Sturgis, J. N. (2006) The photosynthetic apparatus of *Rhodopseudomonas palustris*: Structures and organization. *J. Mol. Biol. 358*, 83–96.
10. Bahatyrova, S., Frese, R. N., Siebert, C. A., Olsen, J. D., Van Der Werf, K. O., Van Grondelle, R., Niederman, R. A., Bullough, P. A., Otto, C., and Hunter, C. N. (2004) The native architecture of a photosynthetic membrane. *Nature 430*, 1058–1062.
11. Scheuring, S., Busselez, J., and Levy, D. (2005) Structure of the dimeric PufX-containing core complex of *Rhodobacter blasticus* by in situ atomic force microscopy. *J. Biol. Chem. 280*, 1426–1431.
12. Goncalves, R. P., Bernadac, A., Sturgis, J. N., and Scheuring, S. (2005) Architecture of the native photosynthetic apparatus of *Phaeospirillum molischianum*. *J. Struct. Biol. 152*, 221–228.
13. Lavergne, J., Vermeglio, A., and Joliot, P. (2008) *Functional coupling between reaction centers and cytochrome bc_1 complexes*, 3rd ed., Springer, Dordrecht, The Netherlands.
14. Scheuring, S., and Sturgis, J. N. (2006) Dynamics and diffusion in photosynthetic membranes from *Rhodospirillum photometricum*. *Biophys. J. 91*, 3707–3717.
15. Mascle-Allemand, C., Lavergne, J., Bernadac, A., and Sturgis, J. N. (2008) Organisation and function of the *Phaeospirillum molischianum* photosynthetic apparatus. *Biochim. Biophys. Acta 1777*, 1552–1559.
16. Konorty, M., Kahana, N., Linaroudis, A., Minsky, A., and Medalia, O. (2008) Structural analysis of photosynthetic membranes by cryo-electron tomography of intact *Rhodopseudomonas viridis* cells. *J. Struct. Biol. 161*, 393–400.
17. Olsen, J. D., Tucker, J. D., Timney, J. A., Qian, P., Vassilev, C., and Hunter, C. N. (2008) The organization of LH2 complexes in membranes from *Rhodobacter sphaeroides*. *J. Biol. Chem. 283*, 30772–30779.
18. Kirchhoff, H. (2008) Molecular crowding and order in photosynthetic membranes. *Trends Plant Sci. 13*, 201–207.
19. Thomas, P. E., Ryan, D., and Levin, W. (1976) An improved staining procedure for the detection of the peroxidase activity of cytochrome p-450 on sodium dodecyl sulfate polyacrylamide gels. *Anal. Biochem. 75*, 168–176.
20. Garcia, A., Vernon, L. P., Ke, B., and Mollenhauer, H. (1968) Some structural and photochemical properties of *Rhodopseudomonas* species NHTC 133 subchromatophore particles obtained by treatment with Triton X-100. *Biochemistry 7*, 326–332.
21. Lang, F. S., and Oesterhelt, D. (1989) Microaerophilic growth and induction of the photosynthetic reaction center in *Rhodopseudomonas viridis*. *J. Bacteriol. 171*, 2827–2834.
22. Dubochet, J., Adrian, M., Chang, J. J., Homo, J. C., Lepault, J., McDowall, A. W., and Schultz, P. (1988) Cryo-electron microscopy of vitrified specimens. *Q. Rev. Biophys. 21*, 129–228.
23. Nickell, S., Forster, F., Linaroudis, A., Net, W. D., Beck, F., Hegerl, R., Baumeister, W., and Plitzko, J. M. (2005) Tom software toolbox: Acquisition and analysis for electron tomography. *J. Struct. Biol. 149*, 227–234.
24. Hegerl, R. (1996) The EM program package: A platform for image processing in biological electron microscopy. *J. Struct. Biol. 116*, 30–34.

25. Frangakis, A. S., and Hegerl, R. (2001) Noise reduction in electron tomographic reconstructions using nonlinear anisotropic diffusion. *J. Struct. Biol. 135*, 239–250.
26. Joliot, P., Beal, D., and Frilley, B. (1980) New spectrophotometric method for studying photosynthetic reactions. *J. Chim. Phys. Phys.-Chim. Biol. 77*, 209–216.
27. Joliot, P., and Joliot, A. (1984) Electron transfer between the two photosystems. I. Flash excitation under oxidizing conditions. *Biochim. Biophys. Acta 765*, 210–218.
28. Miller, K. R., and Jacob, J. S. (1985) The *Rhodopseudomonas viridis* photosynthetic membrane: Arrangement in situ. *Arch. Microbiol. 142*, 333–339.
29. Cully, M. (1990) Isolation und charakterisierung des bc1-komplexes aus *Rhodopseudomonas viridis*. Ph.D. Thesis, The Ludwig-Maximilians University, Munchen Germany.
30. Garcia, A. F., Venturoli, G., Gad'on, N., Fernandez-Velasco, J. G., Melandri, B. A., and Drews, G. (1987) The adaptation of the electron transfer chain of *Rhodopseudomonas capsulata* to different light intensities. *Biochim. Biophys. Acta 890*, 335–345.
31. Knaff, D. B., Willie, A., Long, J. E., Kriauciunas, A., Durham, B., and Millett, F. (1991) Reaction of cytochrome c_2 with photosynthetic reaction centers from *Rhodopseudomonas viridis*. *Biochemistry 30*, 1303–1310.
32. Garcia, D., Richaud, P., and Vermeglio, A. (1993) The photoinduced cyclic electron transfer in whole cells of *Rhodopseudomonas viridis*. *Biochim. Biophys. Acta 1144*, 295–301.
33. Joliot, P., Joliot, A., and Vermeglio, A. (2005) Fast oxidation of the primary electron acceptor under anaerobic conditions requires the organization of the photosynthetic chain of *Rhodobacter sphaeroides* in supercomplexes. *Biochim. Biophys. Acta 1706*, 204–214.
34. Sabaty, M., Jappé, J., Olive, J., and Verméglio, A. (1994) Organization of electron transfer components in *Rhodobacter sphaeroides* forma sp. *Denitrificans* whole cells. *Biochim. Biophys. Acta 1187*, 313–323.
35. Verméglio, A., Joliot, A., and Joliot, P. (1998) Supramolecular organization of the photosynthetic chain in mutants of *Rhodobacter capsulatus* deleted in cytochrome c_2. *Photosynth. Res. 56*, 329–337.
36. Joliot, P., Vermeglio, A., and Joliot, A. (1990) Electron transfer between primary and secondary donors in *Rhodospirillum rubrum*: Evidence for a dimeric association of reaction centers. *Biochemistry 29*, 4355–4361.
37. Chory, J., Donohue, T. J., Varga, A. R., Staehelin, L. A., and Kaplan, S. (1984) Induction of the photosynthetic membranes of *Rhodopseudomonas sphaeroides*: Biochemical and morphological studies. *J. Bacteriol. 159*, 540–454.
38. Bowyer, J. R., Hunter, C. N., Ohnishi, T., and Niederman, R. A. (1985) Photosynthetic membrane development in *Rhodopseudomonas sphaeroides*. Spectral and kinetic characterization of redox components of light-driven electron flow in apparent photosynthetic membrane growth initiation sites. *J. Biol. Chem. 260*, 3295–3304.
39. Niederman, R. A., Mallon, D. E., and Parks, L. C. (1979) Membranes of *Rhodopseudomonas sphaeroides*. Vi. Isolation of a fraction enriched in newly synthesized bacteriochlorophyll alpha-protein complexes. *Biochim. Biophys. Acta 555*, 210–220.
40. Huang, K. C., Mukhopadhyay, R., and Wingreen, N. S. (2006) A curvature-mediated mechanism for localization of lipids to bacterial poles. *PLoS Comput. Biol. 2*, e151.
41. Tauschel, H. D., and Drews, G. (1967) Morphogenesis of thylakoids in *Rhodopseudomonas palustris*. *Arch. Mikrobiol. 59*, 381–404.
42. Cohen-Bazire, G., and Kunisawa, R. (1963) The fine structure of *Rhodospirillum rubrum*. *J. Cell Biol. 16*, 401–419.
43. Drews, G., and Golecki, J. R. (1995) Structure, molecular organization, and biosynthesis of membrane of purple bacteria. In *Anoxygenic photosynthetic bacteria* (Blankenship, R. E., Madigan, M. T., and Bauer, C. E., Eds.) pp 231−257, Kluwer Academic Publishers, Dordrecht, The Netherlands.
44. Oelze, J., and Drews, G. (1969) Die morphogenese des photosyntheseapparates von rhodospirillum rubrum ii. Die kinetik der thylakoidsynthese nach markieurung der membranen mit [2-14c] azetat. *Biochim. Biophys. Acta 173*, 448–455.
45. Chuartzman, S. G., Nevo, R., Shimoni, E., Charuvi, D., Kiss, V., Ohad, I., Brumfeld, V., and Reich, Z. (2008) Thylakoid membrane remodeling during state transitions in *Arabidopsis*. *Plant Cell 20*, 1029–1039.
46. Rozak, P. R., Seiser, R. M., Wacholtz, W. F., and Wise, R. R. (2002) Rapid, reversible alterations in spinach thylakoid appression upon changes in light intensity. *Plant, Cell Environ. 25*, 421–429.
47. Berry, E. A., Huang, L. S., Saechao, L. K., Pon, N. G., Valkova-Valchanova, M., and Daldal, F. (2004) X-ray structure of *Rhodobacter capsulatus* cytochrome bc_1: Comparison with its mitochondrial and chloroplast counterparts. *Photosynth. Res. 81*, 251–275.
48. Stahlberg, H., Muller, D. J., Suda, K., Fotiadis, D., Engel, A., Meier, T., Matthey, U., and Dimroth, P. (2001) Bacterial Na^+-ATP synthase has an undecameric rotor. *EMBO Rep. 2*, 229–233.
49. Scheuring, S., Rigaud, J. L., and Sturgis, J. N. (2004) Variable lh2 stoichiometry and core clustering in native membranes of *Rhodospirillum photometricum*. *EMBO J. 23*, 4127–4133.
50. Voeltz, G. K., and Prinz, W. A. (2007) Sheets, ribbons and tubules: How organelles get their shape. *Nat. Rev. Mol. Cell Biol. 8*, 258–264.
51. Frese, R. N., Olsen, J. D., Branvall, R., Westerhuis, W. H., Hunter, C. N., and van Grondelle, R. (2000) The long-range supraorganization of the bacterial photosynthetic unit: A key role for PufX. *Proc. Natl. Acad. Sci. U.S.A. 97*, 5197–5202.
52. Chandler, D. E., Hsin, J., Harrison, C. B., Gumbart, J., and Schulten, K. (2008) Intrinsic curvature properties of photosynthetic proteins in chromatophores. *Biophys. J. 95*, 2822–2836.
53. Dudkina, N. V., Heinemeyer, J., Keegstra, W., Boekema, E. J., and Braun, H. P. (2005) Structure of dimeric ATP synthase from mitochondria: An angular association of monomers induces the strong curvature of the inner membrane. *FEBS Lett. 579*, 5769–5772.
54. Strauss, M., Hofhaus, G., Schroder, R. R., and Kuhlbrandt, W. (2008) Dimer ribbons of ATP synthase shape the inner mitochondrial membrane. *EMBO J. 27*, 1154–1160.
55. Wynn, R. M., Gaul, D. F., Shaw, R. W., and Knaff, D. B. (1985) Identification of the components of a putative cytochrome bc_1 complex in *Rhodopseudomonas viridis*. *Arch. Biochem. Biophys. 238*, 373–377.
56. Crofts, A. R., and Wraight, C. A. (1983) The electrochemical domain of photosynthesis. *Biochim. Biophys. Acta 726*, 149–185.
57. Joliot, P., Vermeglio, A., and Joliot, A. (1989) Evidence for supercomplexes between reaction centers, cytochrome c_2 and cytochrome bc_1 complex in *Rhodobacter sphaeroides* whole cells. *Biochim. Biophys. Acta 975*, 336–345.
58. Joliot, P., Joliot, A., and Vermeglio, A. (1997) Photo-induced cyclic electron transfer operates in frozen cells of *Rhodobacter sphaeroides*. *Biochim. Biophys. Acta 1318*, 374–384.
59. Jungas, C., Ranck, J. L., Rigaud, J. L., Joliot, P., and Vermeglio, A. (1999) Supramolecular organization of the photosynthetic apparatus of *Rhodobacter sphaeroides*. *EMBO J. 18*, 534–542.
60. Lavergne, J., Joliot, P., and Verméglio, A. (1989) Partial equilibration of photosynthetic electron carriers under weak illumination: A theoretical and experimental study. *Biochim. Biophys. Acta 975*, 346–354.
61. Crofts, A. R. (2000) Photosynthesis in *Rhodobacter sphaeroides*. *Trends Microbiol. 8*, 105–106.
62. Crofts, A. R. (2000) Response from crofts. *Trends Microbiol. 8*, 107–108.
63. Myllykallio, H., Drepper, F., Mathis, P., and Daldal, F. (1998) Membrane-anchored cytochrome c_y mediated microsecond time range electron transfer from the cytochrome bc_1 complex to the reaction center in *Rhodobacter capsulatus*. *Biochemistry 37*, 5501–5510.
64. Myllykallio, H., Drepper, F., Mathis, P., and Daldal, F. (2000) Electron-transfer supercomplexes in photosynthesis and respiration. *Trends Microbiol. 8*, 493–494.
65. Minsky, A., Shimoni, E., and Frenkiel-Krispin, D. (2002) Stress, order and survival. *Nat. Rev. Mol. Cell Biol. 3*, 50–60.